Exploring the regeneration potential of salivary glands using organoids as a model

Rocchi, Cecilia

DOI:
10.33612/diss.168896082

CHAPTER 4

THE HIPPO SIGNALING PATHWAY EFFECTOR YAP REGULATES SALIVARY GLAND REGENERATION AFTER INJURY

Rocchi C., Serrano Martinez P., Jellema - de Bruin A., Baanstra M., Brouwer U., del Angel Zuivre C., Schepers H., van Os R., BarazzuoL L.*, Coppes RP.

Under revision in Science Signalling

ABSTRACT

Adult tissue regeneration involves dynamic cellular processes responsible for restoring tissue integrity. Little is known about how adult salivary gland cells sense and respond to injury. Here, using an *in vivo* injury model and through genetic loss/gain of function approaches in salivary gland-derived organoids, we define a central role for YAP during adult salivary gland regeneration. We show that YAP nuclear activity changes dynamically between homeostasis and regeneration in the salivary gland epithelium. Local injury of the gland triggers a region-specific YAP activation at the regeneration site, characterized by activation of the normally dormant ductal compartment. In a well-defined *in vitro* organoid model, we show that promoting YAP nuclear translocation increases the regenerative ability of human salivary gland-derived cells. Our results point towards a YAP-driven plasticity of the salivary gland ductal compartment during regeneration that could be used to promote *in vivo* regeneration of salivary gland after radiation-induced damage.

INTRODUCTION

Radiotherapy is a major part of the treatment for over 500,000 patients per year that are diagnosed with head and neck cancer worldwide[1]. While radiotherapy treatment significantly increases the survival rate of these patients, the unavoidable inclusion of healthy salivary glands within the radiation field leads to a high probability of developing late radiation toxicity which culminates in the onset of radiation-induced hyposalivation and consequential xerostomia[2-4]. The extent of structural damage and subsequent functional decline of an organ following radiation treatment depends on the cellular radiosensitivity of the given tissue[4]. The salivary gland epithelium is composed of morphologically and functionally distinct cell types and compartments. Similarly to other adult tissue, such as the intestine[5], different compartments of the gland display differential responses, both in terms of kinetics and sensitivity to ionizing radiation[6].

The acinar compartment, the functional unit of the salivary gland, has been shown to be mitotically active, thus playing an important role in the maintenance of adult mouse salivary gland tissue homeostasis[7,8]. Additionally, upon radiation damage, $SOX2^+$ acinar cells show regenerative capacity within the first 30 days post-irradiation[8]. Their regenerative ability, however, appears to be limited and their eventual loss of cell division ability due to radiation-induced damage leads to the loss of the functional acinar compartment[6,8,9]. In contrast, the excretory and striated ductal network compartment, which modifies the saliva composition and directs saliva secretion to the oral cavity, appears to be in a relative quiescent state[10,11]. The slow turnover and the observation that ductal cells show little to no loss of ductal specific marker expression[8] after irradiation may be indicative of a relative resistance to radiation-induced damage, similar to what has been observed for brain cells[12,13].

While some lineage tracing studies in adult mouse salivary glands point towards the existence of mainly progenitor lineage-restricted populations ($K14^+$, $Kit^+/K5^+$) within the ductal compartment[9,14], others point to a possible plasticity of the intercalated and excretory duct compartments in contributing to the regeneration of the functional acinar unit of irradiated glands[15]. However, after high radiation doses these compartments fail to fully regenerate the salivary gland tissue ultimately leading to the functional loss of saliva production[15-17].

Interestingly, we previously showed in both rats and patients, that the radiation dose delivered to the region of the parotid salivary gland containing the main ducts predicts salivary gland dysfunction. This supports the idea of the existence of a stem/progenitor cell population residing in the main ducts and therefore sparing this region has been proposed as a means to preserve saliva production after radiotherapy treatment[18].

Furthermore, *in vitro* 3D culture of salivary gland Wnt-responsive cells showed the ability of $Epcam^{high}$ excretory ductal cells to enter into the cell cycle and give rise to organoids containing terminally differentiated acinar cells, indicating that the appropriate signaling stimulation can

guide the quiescent compartment to an active state able to generate a tissue resembling structure[19]. While Wnt signaling has been shown to drive *in vitro* self-renewal and maintenance of salivary glands, the pathways involved in regeneration of the salivary glands after injury remain poorly understood.

The transcriptional regulator Yes-Associated Protein (YAP) emerged as a key control factor of tissue growth and regeneration in tissue such as intestine, liver and skin[20,21]. YAP transcriptional activity relies on the changes in its nuclear-cytoplasmic localization that is tightly controlled by the Hippo pathway. The Hippo pathway consists of a highly conserved group of serine/threonine kinases that by phosphorylation of YAP at serine 127 determine its cellular localization. The core of the Hippo pathway is composed of MST1 and MST2 kinases which activate the Lats1 and Lats2 kinases to promote YAP phosphorylation. Inactivation of the pathway kinase cascade leads to YAP nuclear translocation and its transcriptional activation by binding to TEA-domain (Tead) family of transcription factors. The ectopic activation of YAP has been shown to promote stem/progenitor cell expansion and to de-differentiate somatic epithelial cells, such as mammary gland and pancreas, to a stem cell state[22] opening important opportunities for regenerative medicine. The ability to increase the stem cell number or transiently activate existing stem cells could be especially important in tissues with a slow turnover or a low regenerative potential, such as the salivary gland[21,23]. YAP function has been examined in the salivary gland and has been implicated in development[24]. Deletion of YAP in the developing salivary gland epithelium leads to severe morphogenesis defects of the glands reflecting compromised epithelial patterning. The inability of YAP-null embryonic salivary gland epithelium to specify ductal progenitors indicates the importance of YAP during the development of salivary glands[24]. However, little is known about where and when YAP is expressed in adult salivary glands[25].

Here we report an essential role of YAP transcriptional activity during homeostasis and regeneration of adult salivary glands after damage. Although YAP has a pivotal role during salivary gland development[24], we show that its activity changes dynamically between homeostasis and regeneration in the adult glands. Upon salivary gland ligation, YAP nuclear expression increases in the ductal compartment at the site of regeneration, supporting the existence of a relatively quiescent stem cell-like population residing in the striated ducts[19]. Using a 3D organoid culture system that has been shown to mimic regeneration[19,26,27], we provide evidence that YAP inactivation diminishes organoid formation efficiency of mouse and human adult salivary gland-derived stem/progenitor cells, while YAP-overexpression promotes stem/progenitor organoid culture expansion. We finally demonstrate that induction of YAP nuclear translocation after irradiation promotes regeneration *in vitro*. Our data further support the idea that regeneration upon severe damage can be mediated by newly activated

ductal cells and that stimulation of YAP nuclear translocation can be used to promote regeneration of radiation-damaged salivary glands.

RESULTS

Increased nuclear YAP expression in salivary gland ductal cells during regeneration

To gain an insight into the role of YAP during adult salivary gland regeneration, an *in vivo* mouse injury model was used to investigate the expression pattern of YAP in adult salivary glands. Both submandibular glands were sutured below the sublingual glands to induce a dynamic regenerative response of the gland. The suture causes the division of the salivary gland into two distinct regions: a lower caudal region of the gland and an upper cranial region (Figure 1A and Supplementary figure 1A and B).

To trace proliferating cells, the mice were subjected to two BrdU injections at 24 and 6 hours prior to sacrifice. Within 14 days of ligation a loss of tissue morphology in the lower caudal region of the gland was evident (Supplementary figure 1B and D). Immunofluorescence staining (IF) showed a pronounced reduction in AQP5 positive acinar cells in the lower caudal region of the gland, while the upper cranial region retained a strong AQP5 expression, indicative of an intact and functional acinar cell compartment (Supplementary figure 1C and D).

Given the pronounced damage that the suture induced to the lower caudal region of the gland, it was next investigated if regeneration was taking place in the upper cranial region of the gland. Interestingly, a significant increase of BrdU positive cells was observed in close proximity to the suture (the regeneration site) (Figure 1B and C and Supplementary figure 1D) compared to the homeostatic area of the gland (distal from the regeneration site) and to the control gland. While the control gland and the homeostatic area of the ligated gland predominantly showed proliferation activity in the intercalated duct and acinar compartments, at the regeneration site proliferation was predominantly in the excretory/striated ductal compartment. These differences in the regenerative response between the cranial and caudal regions of the gland are in accordance with the idea that the ductal compartment contributes to the regeneration of the gland[18].

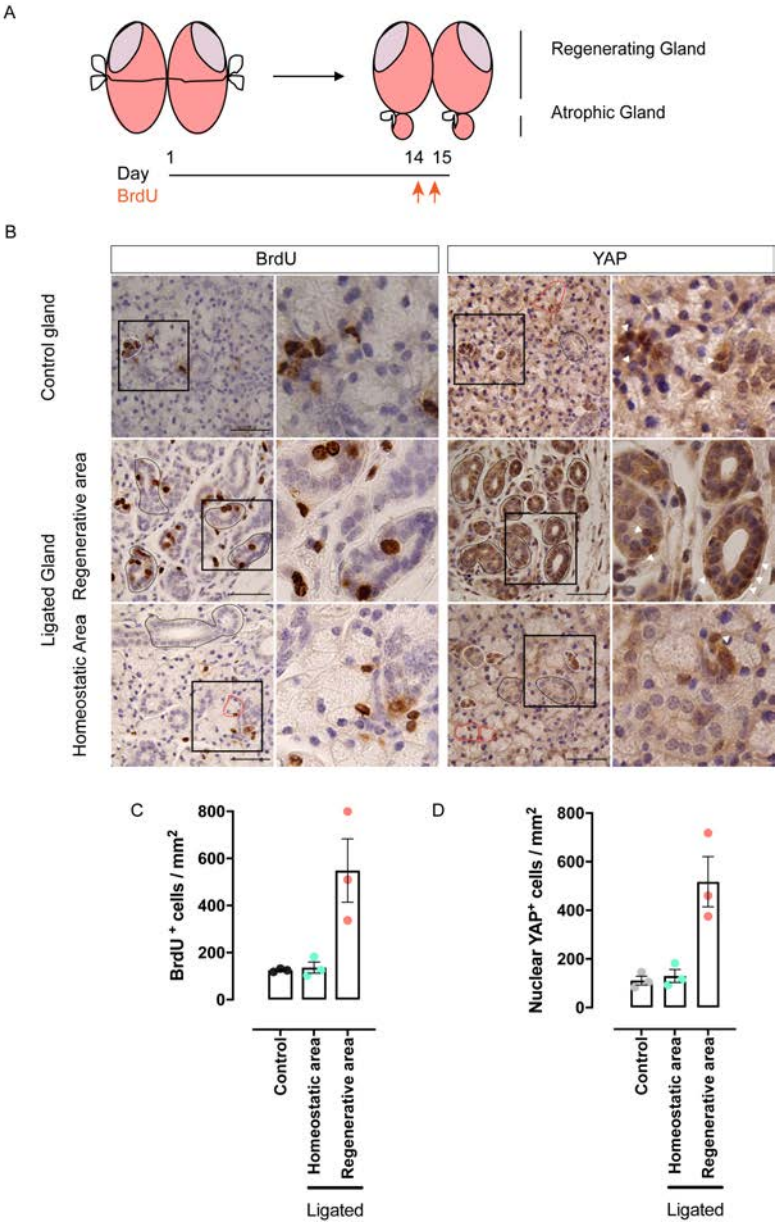

Figure 1: YAP nuclear expression increases in the striated and excretory ductal compartment at the regenerative site of the submandibular gland. (A) Schematic showing the time course of the ligation injury model and BrdU pulses in adult mice. (B) Control and ligated submandibular glands stained at 14 days after ligation for BrdU and total YAP. Intercalated ducts are outlined in white, striated and excretory ducts in black and acinar cells in red. Cells with YAP nuclear localization are indicated by white arrowheads. Scale bars represent 50 μm. (C) Quantification of BrdU positive and (D) nuclear YAP cells per mm^2 of tissue in control homeostatic gland, regenerative and homeostatic areas in ligated gland (see also Supplementary Figure 1B). n=3 for both control glands and ligated glands, were n indicates the number of animals. Each dot represents analysis from a different mouse (n=3). Data are represented as mean ± SEM (C and D). Statistical significance between the three groups was determined using one-way ANOVA ($p<0.05$). *$p<0.05$, **$p<0.01$, ***$p<0.001$, ****$p<0.0001$.

As YAP localization within the cell, nuclear or cytoplasmic, identifies its activity, we examined whether we could observe distinct patterns of YAP protein localization within the ligated

submandibular gland and the control gland. Consecutive submandibular gland sections were analyzed by immunohistochemistry (IHC) against total YAP and BrdU. IHC analysis revealed that YAP expression was predominant in the acinar and intercalated ductal compartments in control salivary glands (Figure 1B), while the excretory ductal compartment, where quiescent stem/progenitor cells have been suggested to reside[19,28], showed a weak cytoplasmic localization of YAP. Interestingly, at two weeks post ligation, IHC of total YAP showed a markedly distinct distribution in the submandibular gland epithelium, with increased nuclear YAP expression in the excretory and striated ductal compartments at the regeneration site and a lower level of nuclear YAP confined predominantly to the acinar intercalated duct compartment in the homeostatic area of the ligated gland (Figure 1B and D and Supplementary figure 1E). The BrdU and YAP expression patterns along the proximal-distal axis of the regeneration site are indicative of a potential dynamic role of YAP during regeneration of the injured gland.

YAP nuclear activity drives mouse salivary gland organoid growth

Given the increased YAP nuclear localization in salivary gland ductal cells during regeneration *in vivo,* we next investigated the function of YAP on self-renewal potential of mouse salivary gland stem/progenitor cells (SGSPCs) as assessed *in vitro* by organoid forming efficiency (OFE). Purified primary ductal cells derived from mouse submandibular glands were seeded in Matrigel and cultured as previously described[19,26]. Treatment with verteporfin (VP), an inhibitor of the YAP-TEAD interaction, at the single cell stage (day 0) completely abrogated organoid formation (Figure 2A-C), whereas drug exposure in 4-day-old organoids led to a collapse of the organoid structure and impairment to form secondary organoids in the next passage (Figure 2D and E; Supplementary figure 2A and B). Similarly, siRNA-mediated YAP knockdown led to a significant decrease of salivary gland OFE (Figure 2F and G). These data suggest an essential role of YAP nuclear activity for SGSPC self-renewal and maintenance. We next reasoned that if inhibition of YAP nuclear activity led to reduced OFE, enhanced YAP nuclear translocation could lead to increased self-renewal potential and expansion of SGSPCs. Indeed, when organoid-derived cells were treated with lysophosphatidic acid (LPA), a compound known to inhibit LATS1/2 kinase activity by modifying cytoskeleton tension[29], simultaneous increase of total YAP protein levels and OFE were observed (Figure 3A-D). To further confirm the importance of YAP nuclear activity in SGSPC self-renewal, we performed siRNA-mediated knock down of LATS1 which resulted in an increased OFE compared to control (Figure 3E-G), further highlighting the importance of Hippo signaling on the activity of SGSPCs.

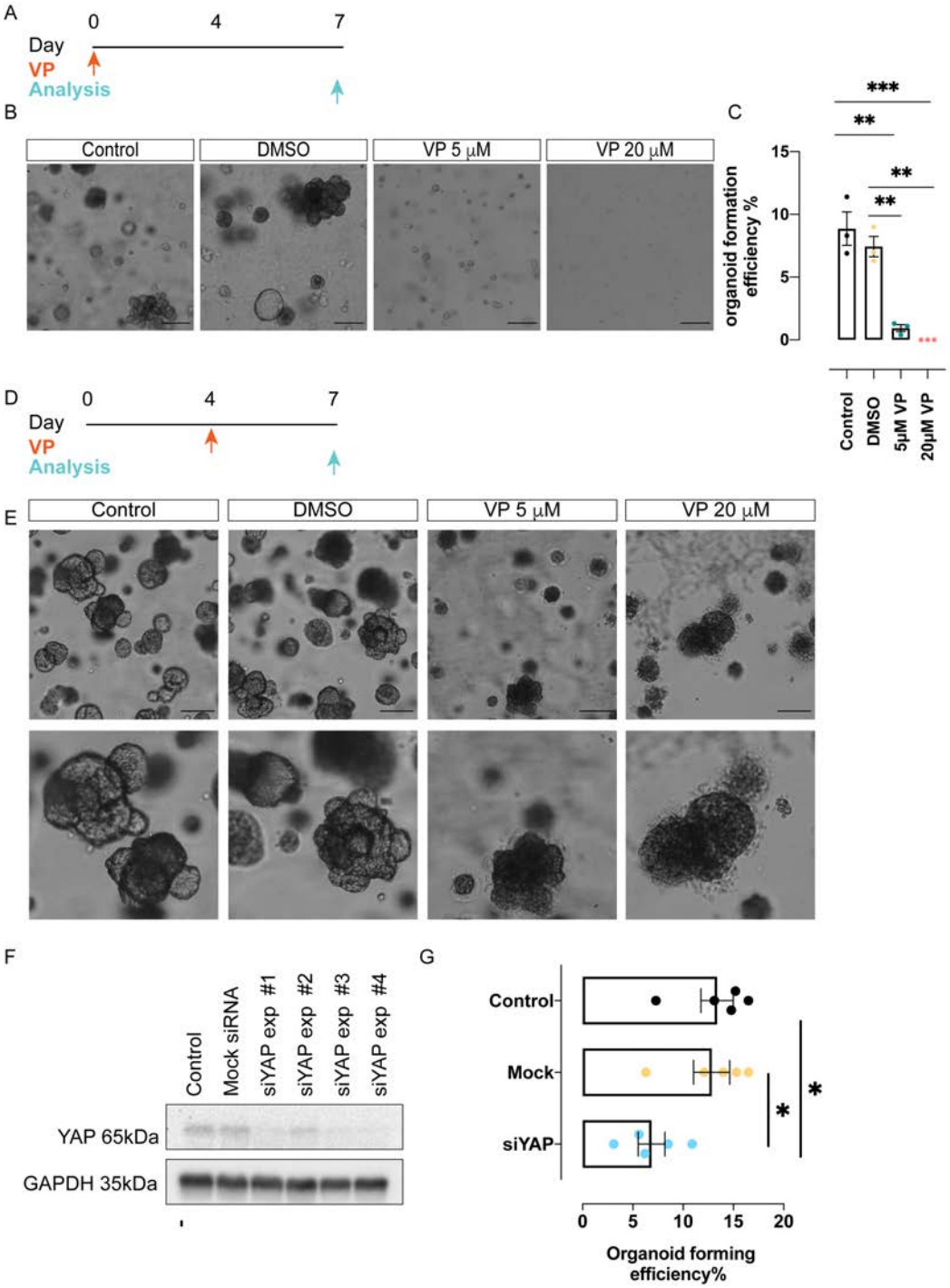

Figure 2: Inhibition of YAP nuclear activity reduces self-renewal ability of mouse adult salivary gland derived stem/progenitor cells. (A)(D) Schematics showing the time course of VP treatment on salivary gland derived organoid culture. (B)(E) Representative images of salivary gland derived organoids treated with DMSO or VP 5 μM and 20 μM respectively from the start of the culture and (B) and from day 4 of culture (E). Scale bar=50 μm. (C) Organoid forming efficiency of mouse salivary gland cells after treatment with VP 5 μM and 20 μM starting at day 0. (F) Western blot analysis of mouse salivary gland organoids showing siYAP knock down efficiency in 4 different experiment (Exp #1 to Exp #4), and (G) their relative ability to form organoids measured as organoid forming efficiency % (OFE%). Mock= scrambled siRNA. Control= no transfection. Data are represented as the mean ± SEM (C)(G). (C)(G) One-way ANOVA was used to test the differences between the groups ($p<0.05$). *$p<0.05$, **$p<0.01$, ***$p<0.001$, ****$p<0.0001$.

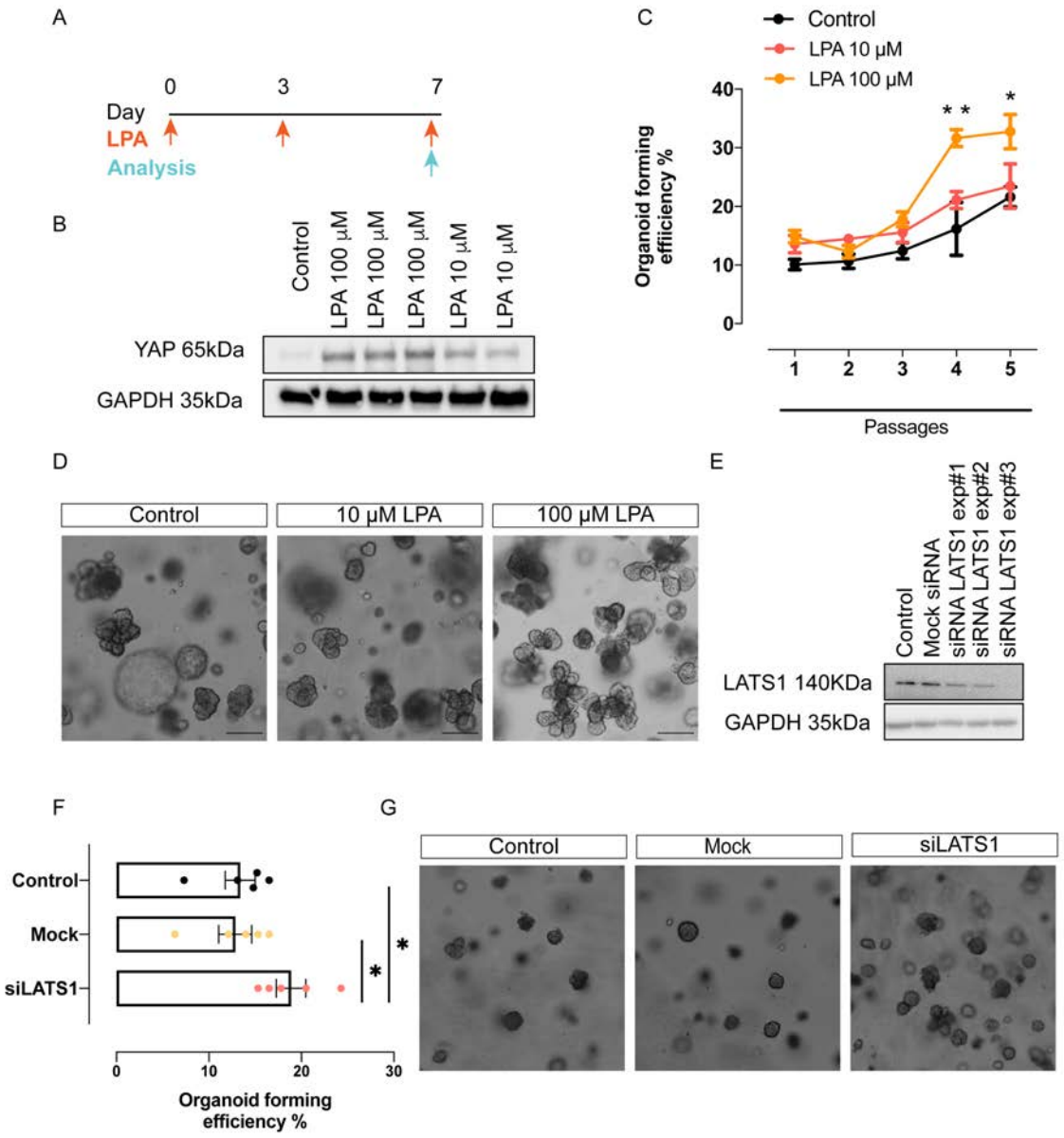

Figure 3: **Stimulation of YAP nuclear translocation increases the ability of salivary gland derived cells to form secondary organoids.** (A) Schematic showing the time line of LPA treatment in salivary gland derived organoid culture. (B) Western blot of lysates from mouse salivary gland derived organoids treated with or without 10 and 100 µM LPA. (C) Organoid formation efficiency of mouse salivary gland derived organoid treated with 10 and 100 µM LPA over 5 passages of culture. (D) Representative pictures of mouse salivary gland organoids at the end of P5 after treatment with 10 and 100 µM LPA. Scale bar=50 µm. (E) Western blot analysis of mouse salivary gland organoids showing siLATS1 knock down efficiency in 3 different experiments (Exp#1 to Exp#3) and (F) their relative ability to form secondary organoids measured as organoid forming efficiency (OFE%). Each dot represents a culture derived from a different mouse (n=4). Mock= scrambled siRNA. Control= no transfection. Data are represented as the mean ± SEM (C)(F). Two-way ANOVA (mixed model) (C); One-way ANOVA (F). *p<0.05, **p<0.01, ***p<0.001, ****p<0.0001.

YAP overexpression in human salivary gland-derived organoids increases stem cell potential

To validate that increased YAP nuclear translocation increases self-renewal ability of SGSPCs, we investigated whether ectopic expression of YAP in salivary gland organoid-derived cells would have similar effects as LPA treatment. We transduced salivary gland organoid-derived cells at the end of passage 1 (P1) with a lentiviral vector encoding for WT YAP-t2A-mCherry[30]. As a control, cells were transduced with an empty lentiviral vector (t2a-mCherry). Transduced cells were cultured for 7 days and, following isolation by fluorescence activated cell sorting for mCherry, plated in Matrigel to assess secondary organoid formation potential (Figure 4A). YAP overexpression was confirmed by western blot analysis of total YAP protein (Figure 4B). Strikingly, YAP overexpressing cells (mCherry+ YAP^{OE}) cultured in EM media gave rise to a significantly higher number of secondary organoids compared to mCherry- and control transduced cells (Supplementary Figure 3A). This difference was maintained for the subsequent 3 passages (Figure 4C and D). We also found that the number of cells and the size of the organoids were significantly increased in YAP^{OE} cells compared to controls (Figure 4E and F). Notably, we observed that overexpression of YAP in human salivary gland-derived organoids cultured in Wnt enriched media (WRYTN) did not support the expansion of the culture to the same extent as in EM media, indicating that YAP and Wnt could have different roles or act at different time during the regeneration process (Supplementary Figure 3B and C). These results indicate that ectopic YAP overexpression promotes stem cell properties in human salivary gland-derived cells. Interestingly, human salivary gland organoids overexpressing YAP cultured in EM media, showed a branched morphology phenotype at the end of P1 which greatly differs from the round shape phenotype of non-overexpressing control organoids and organoids cultured in WRYTN (Supplementary Figure 4A and B). Collectively, several lines of evidence indicate that promoting YAP nuclear translocation increases human SGSPC potential.

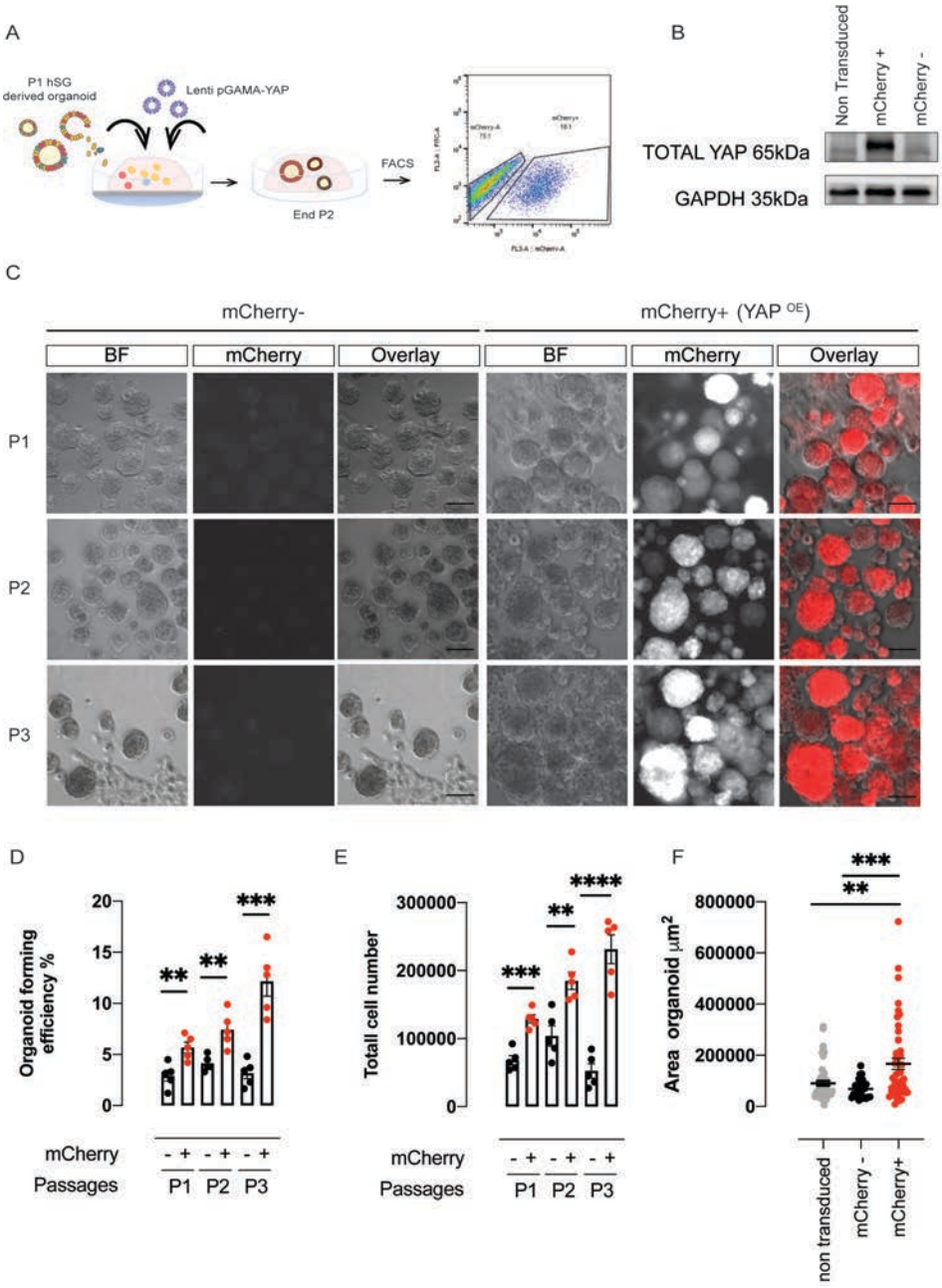

Figure 4: YAP overexpression in human salivary gland derived cells increases their self-renewal potential. (A) Schematic of the experiment performed on human salivary gland (hSG) derived organoids with the lentiviral vector pGAMA-YAP. FACS plot showing the % of mCherry positive cells indicative of the efficiency of transduction. (B) Western blot analysis of lysates derived from hSG transduced organoids showing YAP protein level in non-transduced cells, mCherry- and mCherry+ cells. (C) Representative images and (D) quantification of secondary and tertiary organoids, (E) total cell numbers and (F) area of hSG derived organoid transduced with pGAMA-YAP. Each dot represents a culture derived from a different patient (n=4). Red dots= mCherry+; Black dots= mCherry-. Data are represented as the mean ± SEM (D)(E)(F). One-way ANOVA (D)(E)(F). *p<0.05, **p<0.01, ***p<0.001, ****p<0.0001.

Chemical inhibition of Mst1/2 kinases promotes regeneration of salivary gland organoids after irradiation

The proximal-distal patterning of nuclear YAP from the regeneration site in mouse ligated salivary gland suggests that YAP nuclear activity is required during regeneration. As YAP-overexpression in human SGSPs increases their self-renewal ability, we next investigated whether increased YAP nuclear activity could improve human salivary gland organoid response to irradiation. To increase YAP nuclear translocation upon radiation treatment, we treated human salivary gland organoids with a potent inhibitor of MST1/MST2 kinases (XMU-MP-1), an upstream effector of the Hippo pathway, known to promote liver regeneration after damage[31]. Human SGSP-derived organoids were seeded as single cells in Matrigel and irradiated with 2 and 4 Gy.

Upon irradiation, XMU-MP1-treated cells showed a higher OFE, thus reflecting a higher survival fraction of stem cells after treatment compared to irradiated-only organoids (Figure 5A, Supplementary Figure 5A). Interestingly, the irradiated and XMU-MP1-treated organoids were larger in size than irradiated-only organoids, indicating that after radiation treatment induction of YAP nuclear activity increased proliferation of human SGSPCs and improved the response of human salivary gland organoids to radiation damage (Figure 5B-E). These results indicate that our 3D organoid culture system can be used as a tool to study the underlying signaling pathways responsible for regeneration after radiation-induced damage. It also emphasizes the importance of YAP nuclear translocation as part of the Hippo signaling pathway during regeneration after damage.

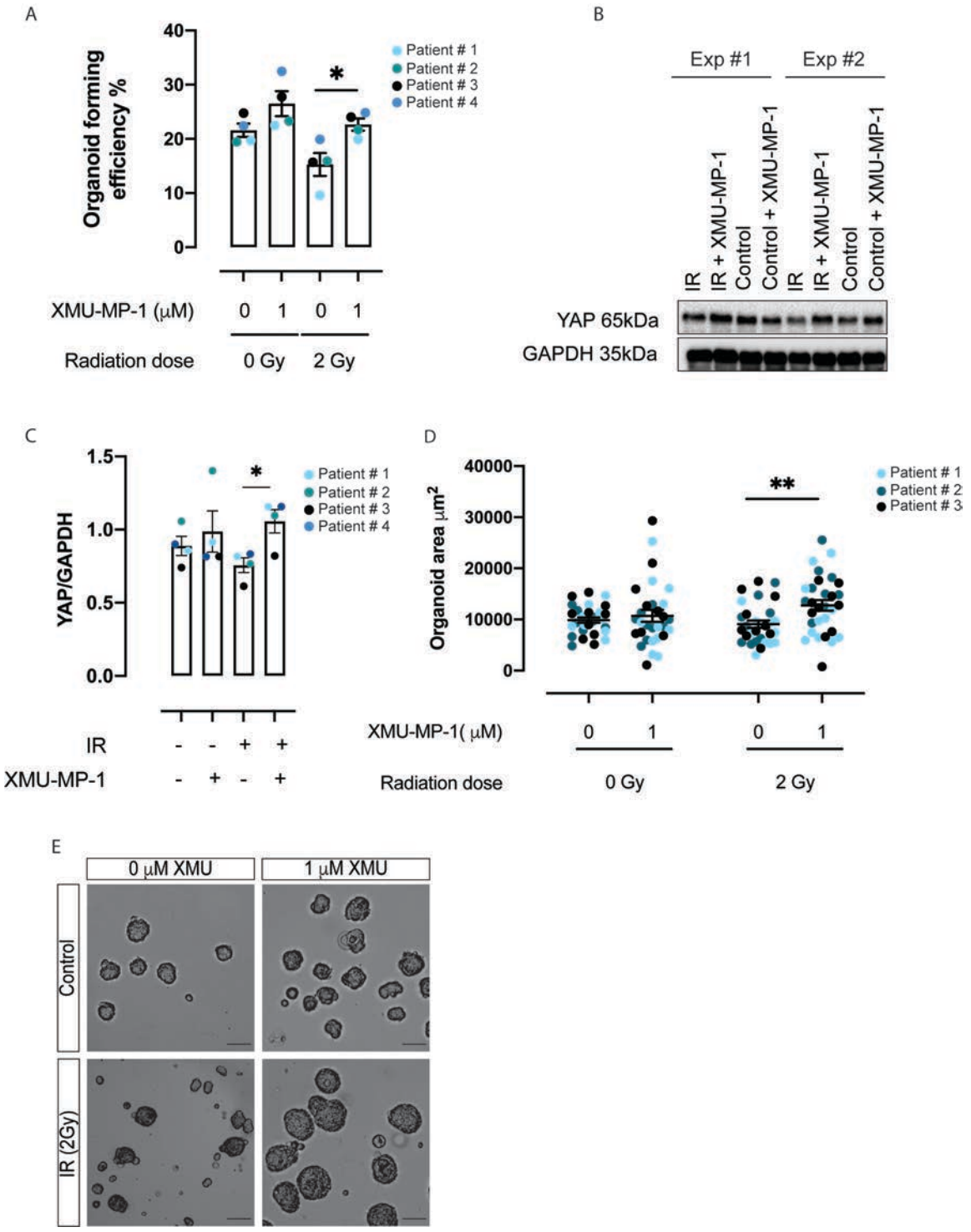

Figure 5: Chemical inhibition of MST1/2 improves salivary gland organoid irradiation response. (A) Organoid forming efficiency and (D) area of hSG derived organoids upon irradiation treatment (2 Gy) and inhibition of MST1/2 kinase by the use of XMU-MP1 (1 μM). Each color represents a culture derived from a different patient (n=4). (B) Western blot analysis of lysates derived from hSG transduced organoids showing changes in total YAP expression upon irradiation and XMU-MP-1 treatment in two different experiments (Exp#1, Exp#2). (C) Quantification of (B). Each color represents a different patient (n=4). (E) Representative images of hSG derived organoid upon irradiation (2 Gy) and XMU-MP-1 (1 μM) treatment. Scale bar=50 μm. Data are represented as the mean ± SEM (A) (C) (D). T-test (C); Two-way ANOVA (mixed model) (A)(C). *p<0.05, **p<0.01, ***p<0.001, ****p<0.0001.

DISCUSSION

Following injury, stem and progenitor cells attempt to re-build both the structural and functional units of the damaged tissue through a tightly controlled process that involves self-renewal and differentiation. While it has been shown that transplantation of SGSPCs can be used to rescue the secretory function of damaged salivary glands[19,26,32,33], the mechanisms of regeneration after injury remain unclear. Here we report that YAP activation is a critical step in the regeneration process of damaged adult salivary glands and modulation of this pathway could be used to increase salivary gland stem cell potential.

We show that during homeostasis salivary glands display low levels of YAP activity, which is confined to the acinar and intercalated ductal compartments known to be involved in the maintenance of the glands[7-9,11,34,35]. After local injury, a dramatic and region-specific increase in nuclear YAP expression was observed at the regeneration site of the ligated gland supporting a role for the Hippo signaling pathway in the response to damage. YAP activation in the normally dormant excretory duct compartment of the salivary gland may point towards the existence in the salivary gland of a 'revival' stem cell population, similar to that seen in the intestine[36], capable of reconstituting the structural and functional unit of the damaged tissue. While differences in regeneration response can be due to the level of damage inflicted to the gland, the ability to regenerate the damaged epithelium by transient YAP activation following ligation-induced damage may indicate that cellular plasticity, rather than a distinct resident population of progenitor cells, might be responsible for the regeneration of the salivary gland after pronounced damage, in contrast to what has been proposed so far in the salivary gland field[8,9].

While future *in vivo* work combining different injury models and lineage tracing could be fundamental to verifying the potential contribution of YAP-activated cells to acinar cell replacement, our *in vitro* data from organoid cultures of salivary gland-derived cells seem to support the regeneration ability of the main striated/excretory ductal cell compartment.

Salivary gland-derived organoid cultures arise from Epcam+ cells of the ductal epithelium compartment[19], known to be quiescent during homeostasis[7]. The ability of these cells to give rise to 3D structures (organoids), which contain all major cell types spatially arranged similarly to the tissue of origin, and to rescue hyposalivation phenotype upon intraglandular transplantation, proves their potential plasticity and regeneration ability. The *in vivo* observations that YAP is involved in salivary gland regeneration are supported by a strong decline in organoid formation efficiency upon YAP knock down. Both promoting YAP nuclear translocation and YAP overexpression showed a pronounced increase in the ability to form secondary and tertiary organoids uncovering a role for YAP in the maintenance of stem/progenitor cells and self-renewal capacity. In agreement with what has recently been shown in intestinal organoids, it is tempting to speculate that salivary gland organoid

development also follows a regenerative model that requires transient YAP activation[27]. Contrary to what was shown in the intestine, but in accordance with the *in vivo* role of YAP in embryonic salivary gland development[24], sustained overexpression of YAP seems to promote the formation of branched organoids. The *in vitro* formation of a branched epithelial ductal network indicates a potential additional function of YAP in patterning and morphogenesis of human adult salivary gland epithelium. While our observation, highlights a role for YAP in directing the expansion and patterning of adult human salivary gland epithelial progenitors, its role in specification and differentiation of salivary gland epithelium is still unknown. Further work is needed to elucidate whether YAP could function as a "gatekeeper" in the salivary gland, marking the boundary between the ductal compartment and the distal acinar compartment, similar to other branching organs[37-39].

Finally, we show that our previously described *in vitro* model can be used to study the regeneration of salivary gland organoids after irradiation, and that stimulating YAP nuclear translocation after irradiation significantly improves the radiation response of human salivary gland-derived cells. Moreover, transient chemical stimulation of YAP nuclear translocation could open new treatment possibilities to promote regeneration or enhance expansion of human SGSPCs *in vitro* for transplantation purposes.

While our study supports the idea of YAP as a sensor of tissue integrity[27] and a key driver in regeneration of both murine and human salivary gland organoids, future studies should elucidate whether modulating YAP levels could induce *in vivo* regeneration, with the aim to use this approach as a regenerative therapy to ameliorate radiation-induced hyposalivation.

METHODS

Mice

Eight to twelve-week-old female C57BL/6 mice were purchased from Envigo. Mice were housed in environmentally controlled rooms, under conventional conditions and fed ad libitum in the Animal Facility of the University Medical Center Groningen. All experiments were performed according to approved institutional animal care and use committee (IACUC) protocols of the University of Groningen (under IVD protocol number 184824-01-001).

Patients

Human non-malignant submandibular gland tissues were obtained from donors after informed consent and Institutional Review Board (IRB) approval during an elective head and neck dissection procedure for the removal of squamous cell carcinoma of the oral cavity at the University Medical Centre Groningen (UMCG) and Medical Centre Leuwaarden (MCL).

Contact for Reagent and Resource Sharing

Further information and requests for resources and reagents should be directed to and will be fulfilled by the corresponding authors, Dr. L. Barazzuol (l.barazzuol@umcg.nl) and Prof. Dr. R.P Coppes (r.p.coppes01@umg.nl).

Mouse submandibular gland ligation

C57BL6 mice were anesthetize with the use of isoflurane. A small incision was made in the neck to visualize the submandibular glands. Each submandibular gland was ligated with the use of (non-dissolvable) wire just below the sublingual gland. Fourteen days later the animals were re-anaesthetized and sacrifice by cervical dislocation. Submandibular glands were isolated, ligation removed and fixed in 4% formaldehyde overnight (ON) at room temperature (RT). Section were used for immunohistochemistry and immunofluorescence (as describe below) to determine the regenerative status of the gland.

Control mice with matching sex and age were subjected to a mock ligation surgery that included isoflurane anesthesia, exposure of the submandibular gland and suture of the incision.

BrdU injection and labelling

To assess proliferation in the ligated submandibular gland as well as the control gland, mice were subjected to two intraperitoneal Bromodeoxyuridine (BrdU; Sigma B5002-1G) injections. BrdU was dissolved in physiologic solution at a concentration of 50 mg/Kg of body weight and injected respectively 24 h and 6 h prior sacrifice. Following BrdU labeling, IHC and quantification was performed as describe below.

Immunohistochemistry and immunofluorescence

All antibodies and reagents used in this study are listed in the Table 1.

Table 1: Antibodies and reagents		
REAGENT or RESOURCE	**Source**	**Identifier**
Antibodies		
Rabbit anti-YAP1	Cell Signaling Technology	#4912
Rat anti-BrdU	Biorad	OBT0030G
Rabbit anti-AQP5	Alomone	AQP-005
Rabbit anti LATS1	Cell Signaling Technology	#9153
Goat anti-rabbit Alexa Fluor 488	Invitrogen	A11008
Donkey anti-mouse Alexa Fluor 594	Invitrogen	A21203
Swine anti-rabbit	Dako	E0431
Polyclonal rabbit anti Rat Immunoglobulins biotinylated	Dako	E0468
Anti -mouse IgG HRP linked	GE healthcare	GENXA931
Anti- rabbit IgG HRP linked	GE healthcare	NA934
Mouse anti-GAPDH	Fitzgerald	
Chemical, Peptides and Recombinant Protein		
1-Oleoyl lysophosphatidic acid sodium salt (LPA)	Tocris- Biotechne	3854
Verteporfin (VP)	Tocris	5305
XMU-MP-1	MedChemExpress	HY-100526
Noggin	Preprotech-Bioconnect	120-10C
A8301	Tocris Bioscience	2939
N2 Supplement	Gibco	17502-048
EGF	Sigma	E9644
FGF2	Preprotech-Bioconnect	100-18B
Dexamethasone	Sigma	d4902-25mg

Insulin	Sigma	I6634-100MG
Y-27632 dihydrochloride Rho-Kinase inhibitor	Bioconnect-Abcam	ab120129
HBSS (Hank's Balanced Salt Solution)	GIBCO	14175-129
BSA (Bovine Serum Albumin)	GIBCO	15260037
Glutamax	ThermoFisher Scientific	35050038
Pen/Strep	Invitrogen	15140-163
DMEM F12 (Dulbecco's modified Eagle's medium: F12)	Gibco/Invitrogen	11320-074
Wnt3a conditioned media	Clvers's lab gift	N/A
R-spondin1 conditioned media	Clvers's lab gift	N/A
Matrigel	Vwr	356235
0.05% Tryosin-EDTA	Invitrogen (Gibco Life Technologies)	25300-096
Dispase	Gibco/Invitrogen	17105-041
Collagenase type II	Gibco/Invitrogen	17101-015
Hyaluronidase	Sigma	H3506-5G
$CaCl_2$	Sigma	C3306 SIGMA
5-Bromo-2′-deoxyuridine (brdu used for mouse injection	Sigma	B5002-1G
FBS (Fetal Bovine Serum)	Greiner	lotnr 11113
DAB (3.3'-diaminobenzide)	Sigma	D4168-50set
DAPI	ThermoFisher Scientific/Pierce	62247
Eukit	Sigma	03989-500 ml
Mounting Medium	DAKO	S3025
Triton X-100	Sigma	X100
Tween-20	Sigma	P1379-500ML

H_2O_2 Peroxidase	Jackson ImmunoResearch Laboratories	011-000-120
Donkey serum	Jackson ImmunoResearch Laboratories	017-000-121
Formaldehyde solution	Sigma	252549-1L
Hematoxylin	Sigma	H3136-25G
TGX Stain-Free™ FastCast™ Acrylamide Kit, 10%	Biorad	1610183
TGX Stain-Free™ FastCast™ Acrylamide Kit, 12%	Biorad	1610185
PEI	Sigma	P3143
Polybrene	Santa Cruz	Sc134220
Lipofectamine 2000	Invitrogen	11668-019
Safil 5/0 polyglycolic acid braided coated absorbable	B. Braun	1048507
Critical Commercial Assay		
Vectastatin® ABC kit	Vector	PK-6100
Experimental Model		
C57BL/6 inbred mice	Envigo	057
Oligonucleotides		
Dharmacon siGENOME siRNA smart pools: YAP1(22601)	Dharmacon	M-046247-01-0005
Dharmacon siGENOME siRNA smart pools: LATS1	Dharmacon	M-063467-01-0005
Dharmacon siGENOME siRNA smart pools: stk3	Dharmacon	M-040440-01-0005 5 nmol
Dharmacon siGENOME siRNA smart pools: stk4	Dharmacon	M-059385-01-0005 5 nmol
pGAMA EMPTY Fw		ctagcgaattctt
pGAMA EMPTY Rev		cgaagaattcg
Recombinant DNA		

psPAX2	Addgene	#12260
pCMV-VSV-G	Addgene	#8454
pGAMA-YAP	Addgene	#74942
p-GAMA-empty	This work	N/A
Software and Algorithms		
Prism 8 (Graphpad Software)		https://www.graphpad.com/scientific-software/prism/
Image J	NIH	https://imagej.nih.gov/ij/

Tissue was isolated and fixed in 4% formaldehyde ON at RT. The tissue was then processed using an automatic tissue processor machine (Leica TP 1020) before standard paraffine embedding. Tissue blocks were sliced in 5 μm section using a rotary microtome (Thermo Fisher HM 340E).

For Light microscopy, sections were dewaxed before heat-activated antigen retrieval using a citric acid buffer containing 0.05% tween 20 (10mM, pH: 6). Section were allowed to cool down for 1h at RT followed by permeabilization on 0,4% Triton X-100 in PBS. For BrdU staining sections were treated with 2,5 M HCl for 25 minutes at RT and neutralized with 0,1 M sodium borate (pH= 8.5) for 5 minutes. Sections were permeabilized in blocking solution (1% BSA, 4% serum and 0.4% Triton X-100 in PBS) and incubate with desired primary antibody ON at 4°C. The day after section were washed thoroughly and quenched in 0.5% H_2O_2 followed by secondary antibody incubation in blocking buffer (1% BSA, 4% donkey serum and 0.4% Triton X-100 in PBS). Vectastatin® ABC kit (Vector labs) was used followed by 3.3'-diaminobenzide (DAB) kit to detect positive staining. Finally, sections were counterstained with Hematoxilin, dehydrated and coverslip mounted using Eukit. Negative controls were generated by omitting primary antibody.

For fluorescence double labelling, heated induced antigen retrieval and DNA denaturation procedure were performed as describe above. Slides were incubated for 1 h at RT in blocking buffer (1% BSA, 4% serum and 0.4% Triton X-100 in PBS) prior incubating in primary antibody solution ON at 4°C. The following day section were washed in PBS 3 times for 10 minutes each, followed by incubation in secondary antibody for 1 h at RT. Finally slides were stained with DAPI (4',6-diamidino-2-phenylindole,dihydrochloride) and mounted using DAKO mounting media. Antibodies used and their final dilutions are as follows: rabbit anti-YAP1 (Cell Signaling), 1:100; rat anti-BrdU (Biorad)1:100; rabbit anti AQP5 (Alomone) 1:200.

Isolation of mouse and human submandibular gland derived cells

Submandibular gland were harvested from healthy adult mice, mechanically digested with the use of gentleMACS dissociator (Milteny) and simultaneously digested in the digestion buffer containing collagenase type II (0.63mg/mL; Gibco), hyaluronidase (0.5 mg/mL, Sigma-Aldrich) and $CaCl_2$ (6.25mM; Sigma-Aldrich) in Hank's Balanced Salt Solution (HBSS) containing 1% bovine serum albumin (BSA; Invitrogen).The digestion procedure was repeated for 2 periods of 30 minutes in a shaking water bath at 37°C. To obtain optimal digestion, both submandibular glands from a single mouse were digested in a 2 mL volume of the digestion buffer. At the end of the digestion, cells were collected by centrifugation at 400 G for 5 minutes and filter through a 100 μm cell strainers (BD Biosciences). The resultant cell suspension was centrifuged at 400 G for 5 minutes and resuspended in Dulbecco's modified Eagle's medium: F12 (DMEM F12) containing Pen/Strep antibiotics (Invitrogen), Glutamax, 20 ng/mL epidermal growth factor (EGF; Sigma Aldrich), 20 ng/mL fibroblast growth factor-2 (Sigma- Aldrich), N2 (Invitrogen), 10 μg/mL insulin (Sigma-Aldrich) and 1 μM dexamethasone (Sigma-Aldrich). Cells were plated at a density of $4x10^4$ cells per well in a 12-well plate and incubate at 37°C and 5% CO_2 for 3 days as floating primary culture.

For human submandibular gland cells isolation, the biopsies collected in the operating room were transferred to the lab in a 50 mL falcon tube containing HBSS 1% BSA on ice. The biopsy was weighted in a sterile petri dish and using a sterile disposable scalpel minced into small pieces. To obtain optimal digestion 20 mg of tissue was processed per 1 mL of digestion buffer volume, with a maximum of 100 mg of tissue per tube. The human biopsies were then processed in the same manner as the mouse tissue.

Self-renewal assay of mouse and human salivary gland derived cells

Three days-old primary spheres were harvested and dispersed to single cells suspension using 0.05% trypsin EDTA (Invitrogen). Single cells were counted and resuspended in culture media at a final concentration of $0.4x10^6$ or $0.8x10^6$ cells per mL. 25 μL of cell suspension was mix on ice with 50 μL of ice cold Matrigel and the 75 μL gel pipetted in the middle of a 12-well plate. After solidifying the Matrigel gels were covered in enriched media (EM; DMEM/F12, pen/strep [1x; Invitrogen], glutamax [1x; Invitrogen], N2 [1x; Gibco], EGF [20ng/mL; Sigma Aldrich], FGF2 [20ng/nL;sigma Aldrich], insulin [10μg/mL;Sigma Aldrich], dexamethasone [1μM; Sigma Aldrich], Y27632 [10μM; Sigma Aldrich] or WRYTN (DMEM/F12, pen/strep [1x; Invitrogen], glutamax [1x; Invitrogen], N2 [1x; Gibco], EGF [20ng/mL; Sigma Aldrich], FGF2 [20ng/nL;sigma Aldrich], insulin [10μg/mL;Sigma Aldrich], dexamethasone [1μM; Sigma Aldrich], noggin[50ng/mL; Preprotech-Bioconnect], A8301[1μM Tocris], Y27632 [10μM; Sigma Aldrich], 10% R-spondin1 conditioned medium and 50 % Wnt3a conditioned medium)

media. One week after seeding (end of the passage), the media was replaced with Dispase enzyme (1 mg/mL in DEMEM F12 at 37°C for 30-45 minutes) to dissolve the gels. All the organoids released from the dissolved gels were processed to single cells using 0.05% trypsin-EDTA treatment to form single cell suspension. Organoids and cell number at the end of the passage were noted and the secondary organoid derived single cells re-seeded in Matrigel to start a new passage. Number of organoids and single cells at the end of each passage were used to calculate Organoid Formation Efficiency percentage (OFE%) and Population Doubling as follows:

$$Organoid\ Formation\ Efficiency\ (OFE\%) = \frac{Number\ of\ Organoid\ harvested\ at\ the\ end\ of\ the\ pasaage}{Number\ of\ single\ cells\ seeded\ at\ the\ beginning\ of\ the\ passage}\ x\ 100$$

$$Population\ Doubling = \frac{\ln(harvestes\ cells/seeded\ cells)}{ln2}$$

Irradiation treatment of mouse salivary gland-derived cells

Photon irradiation of 3-day-old salivary gland derived organoid seeded in Matrigel was performed with ^{137}Cs source (IBL 637 Cesium-137 γ-ray machine) with a dose rate of 0.59 Gy/min.

Drug treatment of mouse and human salivary gland-derived cells

To modulate YAP activity during mouse salivary gland-derived organoid growth, cells were culture in WRY (DMEM/F12, pen/strep [1x; Invitrogen], glutamax [1x; Invitrogen], N2 [1x; Gibco], EGF [20ng/mL; Sigma Aldrich], FGF2 [20ng/nL;sigma Aldrich], insulin [10μg/mL;Sigma Aldrich], dexamethasone [1μM; Sigma Aldrich], Y27632 [10μM; Sigma Aldrich], 10% R-spondin1 conditioned medium and 50 % Wnt3a conditioned medium). For YAP nuclear activity inhibition mouse organoid were culture in WRY containing 5 or 20 μM of Verteporfin. Drug was added at day 0 or at day 4 of culture and media refreshed every 2 days. Control culture were cultured in WRY containing the same % of DMSO. To promote YAP nuclear translocation, lysophosphatidic acid (LPA) was added to mouse organoid culture at a final concentration of 10 or 100 μM from day 0. Media was refreshed every 3 days.

To promote YAP nuclear translocation in human salivary gland-derived organoid culture, single cells were seeded in Matrigel and cultured in WRYTN media. Immediately after irradiation, XMU-MP-1 was added to the wells at a final concentration of 1 or 3μM. Media was changed every 2 days.

siRNA transfection of mouse salivary gland-derived cells

Mouse salivary gland derived-cells were transfected using siGENOME SMART pool siRNAYAP, siRNALATS1 and Non-Targeting siRNA from Dharmacon. Cells were seeded at a density of 1 to $1.5x10^5$ in a 12-well plate and incubated at 37°C and 5% CO_2. The second day transfection was done using Lipofectamine 2000 (Invitrogen) in antibiotic-free medium according to manufacturer instructions. Five hours post transfection media was replaced with EM culture media and cells incubate at 37°C and 5% CO_2. A second round of transfection was performed and 5 h post transfection cells were counted, resuspended in EM culture media at a density $0.8x10^6$ cells/mL and seeded in Matrigel. 72 h from the first transfection cells were harvested to check efficiency of knock down. At the end of the passage organoids and cells were counted to establish the OFE%.

Lentiviral production

$1.5x10^6$ HEK293T cells were plated in poly-L-lysin coated 10 cm dish in DMEM supplemented with 10% FBS, Pen/Strep [1x; Invitrogen], Glutamax [1x; Invitrogen] and incubated ON at 37°C and 5% CO_2. On the next day cells were transfected with 3 μg of p-GAMA YAP (AddGene)[30] or empty p-GAMA 3 μg of the packaging plasmid PAX2, 0.7 μg of envelope plasmid VSV-G and 40 μL of PEI (1 μg/mL) as previously described[40]. On the next day medium was changed to DMEM F12. Two days after transfection the viruses were collected, filtered through a sterile syringe filter with a 0.45 μm pore size and hydrophilic PVDF membrane and frozen in 250 μL aliquots at -80 °C. We have tittered the virus-containing supernatant by transduction of mCherry gene. Viruses were always in the range of $5.0x10^6$ – $7.0x10^6$ transduction unit (TU)/mL.

Lentiviral transduction and cell sorting of human salivary gland-derived cells.

Human salivary gland-derived organoids at the end of passage 1 (P1) were released from Matrigel and dissociated to single cells using 0.05% trypsin-EDTA (Invitrogen). Human salivary gland organoid-derived single cells were counted and resuspended in WRYTN media to a final concentration of $2.5x10^6$ cells per mL. For each 100 μL of cell suspension 250 μL of viral supernatant and polybrene (6 μg/mL) was added. The mixture was divided in 350 μL aliquots in a 24-well plate and incubated ON at 37°C and 5% CO_2. The day after transduction single cells were counted to adjust for dead cells, resuspended in media to a final concentration of $0.8x10^6$ cells per mL and seeded in Matrigel into 12-well plate. The cells were cultured for 7 to 10 days in WRYTN media at 37°C and 5% CO_2. At day 7 (or day 10) Matrigel was dissolved with the use of Dispase enzyme (1 mg/mL), and organoids dispersed to single cells with the use of 0.05% trypsin-EDTA. Cells were washed with 0.2% BSA in PBS and

resuspended in 0.2% BSA with the viability dye (DAPI) in PBS. YAP overexpressing cells were isolated by fluorescence-activated cell sorting for mCherry-positive cells, seeded in Matrigel and cultured in WRYTN for the next 3 passages.

Immunoblot

To monitor endogenous gene responses, mouse and human organoids were harvested and centrifuged pellets homogenized by sonication in 2x Laemnli buffer. Protein concentration of the lysates was determined using Bradford quantification method. Homogenates were then boiled at 99°C for 5 minutes and equal protein amounts were separated with 10 or 12% polyacrylamide gels and transfered to PVDF membranes using Trans Blot Turbo System (Bio-Rad). The membranes were blocked in 5% BSA in PBS-Teween-20 and incubated 1 h at RT. Incubation with primary antibodies was done ON at 4°C following by incubation with HRP-conjugated secondary antibodies. Membranes were developed using ECL reagent (Thermo Fisher Scientific) and the signal was detected using ChemiDoc imager (Biorad). Densiometric analysis of western blots at non-saturated exposure were performed using Image J software and the values normalized against the one of GAPDH loading control. For immunoblots, the following primary antibodies at the indicated dilutions were used: rabbit anti-YAP (Cell Signaling) 1:1000; rabbit anti-LATS1 (Cell Signaling) 1:1000; mouse anti-GAPDH (Fitzgerald) 1:10000.

Quantification of IHC images

Light microscopy images taken at 40x, were quantitatively analysed for BrdU and YAP nuclear expression with the use of ImageJ (NIH) software. Five areas (309.68 μm x 232.26 μm) were chosen within each regenerative and homeostatic area of the ligated and control glands, from 3 biological replicates (n=3). For each replicate three different sections were analysed. To quantify the nuclear localization of BrdU or YAP, for each picture, positive nuclear were manually counted using Image J software and the means of positive nuclear/mm^2 calculated and plotted with the use of GraphPad Prism8.

Statistical Analysis

All statistical analyses in this study were performed using GraphPad Prism8 software (GraphPad, La Jolla, CA, USA). The number of mice, patients or individual organoids analyzed (n), presented error bars (SEM), statistical analysis and p values are all stated in each figure or figure legend.

REFERENCES

1 Siegel, R. L., Miller, K. D. & Jemal, A. Cancer statistics, 2018. *CA Cancer J Clin* **68**, 7-30, doi:10.3322/caac.21442 (2018).

2 Vissink, A., Jansma, J., Spijkervet, F. K., Burlage, F. R. & Coppes, R. P. Oral sequelae of head and neck radiotherapy. *Crit Rev Oral Biol Med* **14**, 199-212, doi:10.1177/154411130301400305 (2003).

3 Grundmann, O., Mitchell, G. C. & Limesand, K. H. Sensitivity of salivary glands to radiation: from animal models to therapies. *J Dent Res* **88**, 894-903, doi:10.1177/0022034509343143 (2009).

4 Barnett, G. C., West, C. M., Dunning, A. M., Elliott, R. M., Coles, C. E., Pharoah, P. D. *et al.* Normal tissue reactions to radiotherapy: towards tailoring treatment dose by genotype. *Nat Rev Cancer* **9**, 134-142, doi:10.1038/nrc2587 (2009).

5 Metcalfe, C., Kljavin, N. M., Ybarra, R. & de Sauvage, F. J. Lgr5+ stem cells are indispensable for radiation-induced intestinal regeneration. *Cell Stem Cell* **14**, 149-159, doi:10.1016/j.stem.2013.11.008 (2014).

6 Konings, A. W., Coppes, R. P. & Vissink, A. On the mechanism of salivary gland radiosensitivity. *Int J Radiat Oncol Biol Phys* **62**, 1187-1194, doi:10.1016/j.ijrobp.2004.12.051 (2005).

7 Aure, M. H., Konieczny, S. F. & Ovitt, C. E. Salivary gland homeostasis is maintained through acinar cell self-duplication. *Dev Cell* **33**, 231-237, doi:10.1016/j.devcel.2015.02.013 (2015).

8 Emmerson, E., May, A. J., Berthoin, L., Cruz-Pacheco, N., Nathan, S., Mattingly, A. J. *et al.* Salivary glands regenerate after radiation injury through SOX2-mediated secretory cell replacement. *EMBO Mol Med* **10**, doi:10.15252/emmm.201708051 (2018).

9 May, A. J., Cruz-Pacheco, N., Emmerson, E., Gaylord, E. A., Seidel, K., Nathan, S. *et al.* Diverse progenitor cells preserve salivary gland ductal architecture after radiation-induced damage. *Development* **145**, doi:10.1242/dev.166363 (2018).

10 Peter, B., Van Waarde, M. A., Vissink, A., s-Gravenmade, E. J. & Konings, A. W. Radiation-induced cell proliferation in the parotid and submandibular glands of the rat. *Radiat Res* **140**, 257-265 (1994).

11 Kimoto, M., Yura, Y., Kishino, M., Toyosawa, S. & Ogawa, Y. Label-retaining cells in the rat submandibular gland. *J Histochem Cytochem* **56**, 15-24, doi:10.1369/jhc.7A7269.2007 (2008).

12 Barazzuol, L., Ju, L. & Jeggo, P. A. A coordinated DNA damage response promotes adult quiescent neural stem cell activation. *PLoS Biol* **15**, e2001264, doi:10.1371/journal.pbio.2001264 (2017).

13 Kalamakis, G., Brune, D., Ravichandran, S., Bolz, J., Fan, W., Ziebell, F. *et al.* Quiescence Modulates Stem Cell Maintenance and Regenerative Capacity in the Aging Brain. *Cell* **176**, 1407-1419 e1414, doi:10.1016/j.cell.2019.01.040 (2019).

14 Kwak, M., Alston, N. & Ghazizadeh, S. Identification of Stem Cells in the Secretory Complex of Salivary Glands. *J Dent Res* **95**, 776-783, doi:10.1177/0022034516634664 (2016).

15 Weng, P. L., Aure, M. H., Maruyama, T. & Ovitt, C. E. Limited Regeneration of Adult Salivary Glands after Severe Injury Involves Cellular Plasticity. *Cell Rep* **24**, 1464-1470 e1463, doi:10.1016/j.celrep.2018.07.016 (2018).

16 Sullivan, C. A., Haddad, R. I., Tishler, R. B., Mahadevan, A. & Krane, J. F. Chemoradiation-induced cell loss in human submandibular glands. *Laryngoscope* **115**, 958-964, doi:10.1097/01.MLG.0000163340.90211.87 (2005).
17 Marmary, Y., Adar, R., Gaska, S., Wygoda, A., Maly, A., Cohen, J. *et al.* Radiation-Induced Loss of Salivary Gland Function Is Driven by Cellular Senescence and Prevented by IL6 Modulation. *Cancer Res* **76**, 1170-1180, doi:10.1158/0008-5472.CAN-15-1671 (2016).
18 van Luijk, P., Pringle, S., Deasy, J. O., Moiseenko, V. V., Faber, H., Hovan, A. *et al.* Sparing the region of the salivary gland containing stem cells preserves saliva production after radiotherapy for head and neck cancer. *Sci Transl Med* **7**, 305ra147, doi:10.1126/scitranslmed.aac4441 (2015).
19 Maimets, M., Rocchi, C., Bron, R., Pringle, S., Kuipers, J., Giepmans, B. N. *et al.* Long-Term In Vitro Expansion of Salivary Gland Stem Cells Driven by Wnt Signals. *Stem Cell Reports* **6**, 150-162, doi:10.1016/j.stemcr.2015.11.009 (2016).
20 Yui, S., Azzolin, L., Maimets, M., Pedersen, M. T., Fordham, R. P., Hansen, S. L. *et al.* YAP/TAZ-Dependent Reprogramming of Colonic Epithelium Links ECM Remodeling to Tissue Regeneration. *Cell Stem Cell* **22**, 35-49 e37, doi:10.1016/j.stem.2017.11.001 (2018).
21 Moya, I. M. & Halder, G. Hippo-YAP/TAZ signalling in organ regeneration and regenerative medicine. *Nat Rev Mol Cell Biol* **20**, 211-226, doi:10.1038/s41580-018-0086-y (2019).
22 Panciera, T., Azzolin, L., Fujimura, A., Di Biagio, D., Frasson, C., Bresolin, S. *et al.* Induction of Expandable Tissue-Specific Stem/Progenitor Cells through Transient Expression of YAP/TAZ. *Cell Stem Cell* **19**, 725-737, doi:10.1016/j.stem.2016.08.009 (2016).
23 Gregorieff, A., Liu, Y., Inanlou, M. R., Khomchuk, Y. & Wrana, J. L. Yap-dependent reprogramming of Lgr5(+) stem cells drives intestinal regeneration and cancer. *Nature* **526**, 715-718, doi:10.1038/nature15382 (2015).
24 Szymaniak, A. D., Mi, R., McCarthy, S. E., Gower, A. C., Reynolds, T. L., Mingueneau, M. *et al.* The Hippo pathway effector YAP is an essential regulator of ductal progenitor patterning in the mouse submandibular gland. *Elife* **6**, doi:10.7554/eLife.23499 (2017).
25 Chibly, A. M., Wong, W. Y., Pier, M., Cheng, H., Mu, Y., Chen, J. *et al.* aPKCzeta-dependent Repression of Yap is Necessary for Functional Restoration of Irradiated Salivary Glands with IGF-1. *Sci Rep* **8**, 6347, doi:10.1038/s41598-018-24678-4 (2018).
26 Nanduri, L. S., Baanstra, M., Faber, H., Rocchi, C., Zwart, E., de Haan, G. *et al.* Purification and ex vivo expansion of fully functional salivary gland stem cells. *Stem Cell Reports* **3**, 957-964, doi:10.1016/j.stemcr.2014.09.015 (2014).
27 Serra, D., Mayr, U., Boni, A., Lukonin, I., Rempfler, M., Challet Meylan, L. *et al.* Self-organization and symmetry breaking in intestinal organoid development. *Nature* **569**, 66-72, doi:10.1038/s41586-019-1146-y (2019).
28 Pringle, S., Van Os, R. & Coppes, R. P. Concise review: Adult salivary gland stem cells and a potential therapy for xerostomia. *Stem Cells* **31**, 613-619, doi:10.1002/stem.1327 (2013).
29 Yu, F. X., Zhao, B., Panupinthu, N., Jewell, J. L., Lian, I., Wang, L. H. *et al.* Regulation of the Hippo-YAP pathway by G-protein-coupled receptor signaling. *Cell* **150**, 780-791, doi:10.1016/j.cell.2012.06.037 (2012).

30 Qin, H., Hejna, M., Liu, Y., Percharde, M., Wossidlo, M., Blouin, L. *et al.* YAP Induces Human Naive Pluripotency. *Cell Rep* **14**, 2301-2312, doi:10.1016/j.celrep.2016.02.036 (2016).
31 Fan, F., He, Z., Kong, L. L., Chen, Q., Yuan, Q., Zhang, S. *et al.* Pharmacological targeting of kinases MST1 and MST2 augments tissue repair and regeneration. *Sci Transl Med* **8**, 352ra108, doi:10.1126/scitranslmed.aaf2304 (2016).
32 Nanduri, L. S., Lombaert, I. M., van der Zwaag, M., Faber, H., Brunsting, J. F., van Os, R. P. *et al.* Salisphere derived c-Kit+ cell transplantation restores tissue homeostasis in irradiated salivary gland. *Radiother Oncol* **108**, 458-463, doi:10.1016/j.radonc.2013.05.020 (2013).
33 Pringle, S., Maimets, M., van der Zwaag, M., Stokman, M. A., van Gosliga, D., Zwart, E. *et al.* Human Salivary Gland Stem Cells Functionally Restore Radiation Damaged Salivary Glands. *Stem Cells* **34**, 640-652, doi:10.1002/stem.2278 (2016).
34 Kim, Y. J., Kwon, H. J., Shinozaki, N., Hashimoto, S., Shimono, M., Cho, S. W. *et al.* Comparative analysis of ABCG2-expressing and label-retaining cells in mouse submandibular gland. *Cell Tissue Res* **334**, 47-53, doi:10.1007/s00441-008-0667-8 (2008).
35 Chibly, A. M., Querin, L., Harris, Z. & Limesand, K. H. Label-retaining cells in the adult murine salivary glands possess characteristics of adult progenitor cells. *PLoS One* **9**, e107893, doi:10.1371/journal.pone.0107893 (2014).
36 Ayyaz, A., Kumar, S., Sangiorgi, B., Ghoshal, B., Gosio, J., Ouladan, S. *et al.* Single-cell transcriptomes of the regenerating intestine reveal a revival stem cell. *Nature* **569**, 121-125, doi:10.1038/s41586-019-1154-y (2019).
37 Mahoney, J. E., Mori, M., Szymaniak, A. D., Varelas, X. & Cardoso, W. V. The hippo pathway effector Yap controls patterning and differentiation of airway epithelial progenitors. *Dev Cell* **30**, 137-150, doi:10.1016/j.devcel.2014.06.003 (2014).
38 Mamidi, A., Prawiro, C., Seymour, P. A., de Lichtenberg, K. H., Jackson, A., Serup, P. *et al.* Mechanosignalling via integrins directs fate decisions of pancreatic progenitors. *Nature* **564**, 114-118, doi:10.1038/s41586-018-0762-2 (2018).
39 Rosado-Olivieri, E. A., Anderson, K., Kenty, J. H. & Melton, D. A. YAP inhibition enhances the differentiation of functional stem cell-derived insulin-producing beta cells. *Nat Commun* **10**, 1464, doi:10.1038/s41467-019-09404-6 (2019).
40 Schepers, H., van Gosliga, D., Wierenga, A. T., Eggen, B. J., Schuringa, J. J. & Vellenga, E. STAT5 is required for long-term maintenance of normal and leukemic human stem/progenitor cells. *Blood* **110**, 2880-2888, doi:10.1182/blood-2006-08-039073 (2007).

ACKNOWLEDGMENTS

This work was supported by grant from the Dutch Cancer Society (RUG 2013-5792).

We would like to thank the maxillofacial surgical team of the University Medical Center Groningen and Medical Center Leeuwarden for providing donor biopsies and Monique Stokman for coordination of the sampling of donor material. We also thank the staff members of the Department of Biomedical Sciences of Cells & Systems of the University Medical Center of Groningen for fruitful discussion of data.

AUTHOR CONTRIBUTIONS

C.R. conceptualized the study, designed and performed the experiments, analyzed and interpreted data, wrote and edited the paper. P.S.M. and U.B. contributed to the animal ligation experiments. A.J.d.B. and M.B. contributed to the mouse and human *in vitro* experiments (culture and FACS). C.d.A.Z. contributed to the mouse *in vitro* experiments. H.S. contributed to the conceptualization of the lentiviral experiments, interpretation of the data as well as manuscript writing. R.v.O. and L.B. contributed to the conceptualization, data analysis and interpretation, as well as the design and manuscript writing. R.P.C. provided financial support, contributed to the conceptualization, data analysis and interpretation as well as the design and manuscript writing.

SUPPLEMENTARY INFORMATION

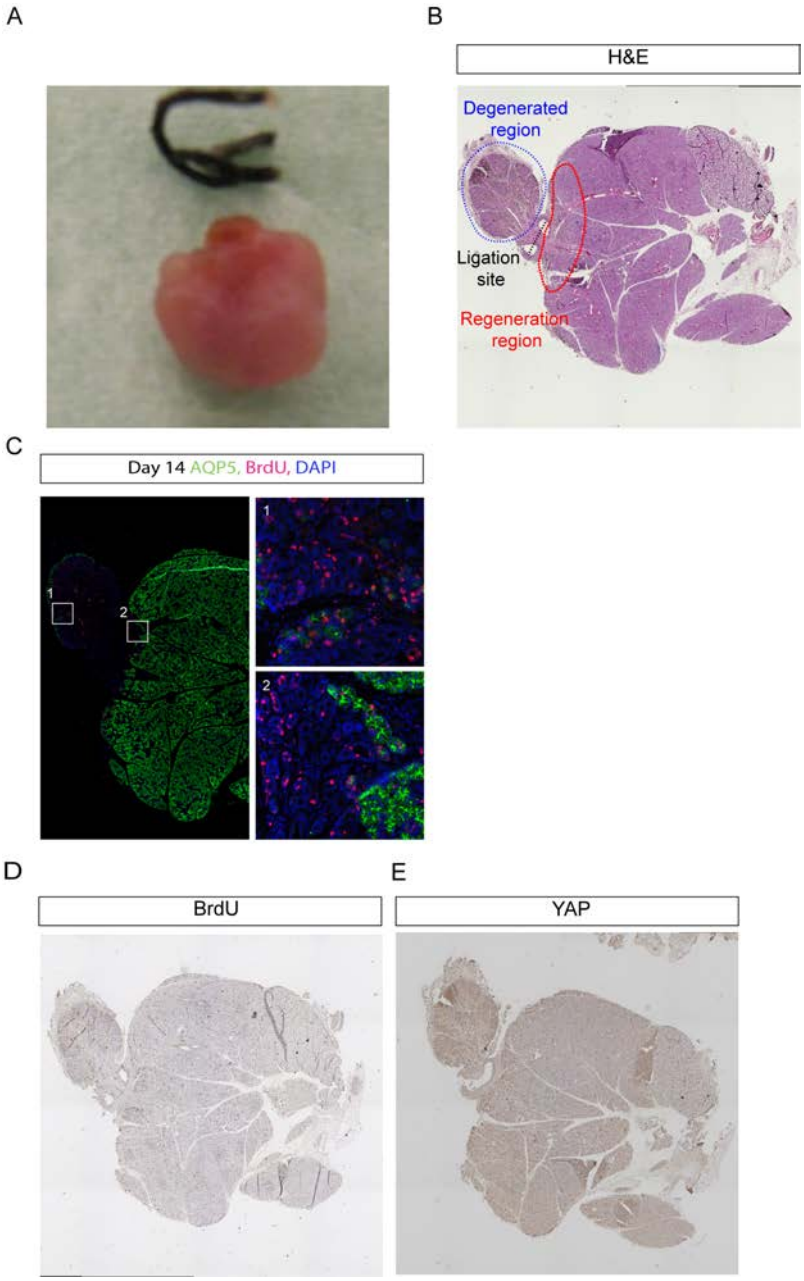

Supplementary Figure 1: YAP nuclear expression increases in the striated and excretory ductal compartment at the regenerative site of the submandibular gland. Relative to Figure 1. (A) Picture showing a mouse salivary gland 14 days after ligation. (B and E) Establishment and characterization of ligated mouse submandibular glands. (B) H&E tile scan showing the ligation site (black dashed line), the degenerative region of the gland (blue dashed line) and the regeneration region of the gland (red dashed line). (C) Immunofluorescent staining of mouse ligated submandibular gland 14 days after ligation. In green aquaporin 5 (AQP5), in red BrdU. White box insets (1 and 2) represent the regions of magnifications. (D) IHC of consecutive paraffine sections showing BrdU and (E) YAP.

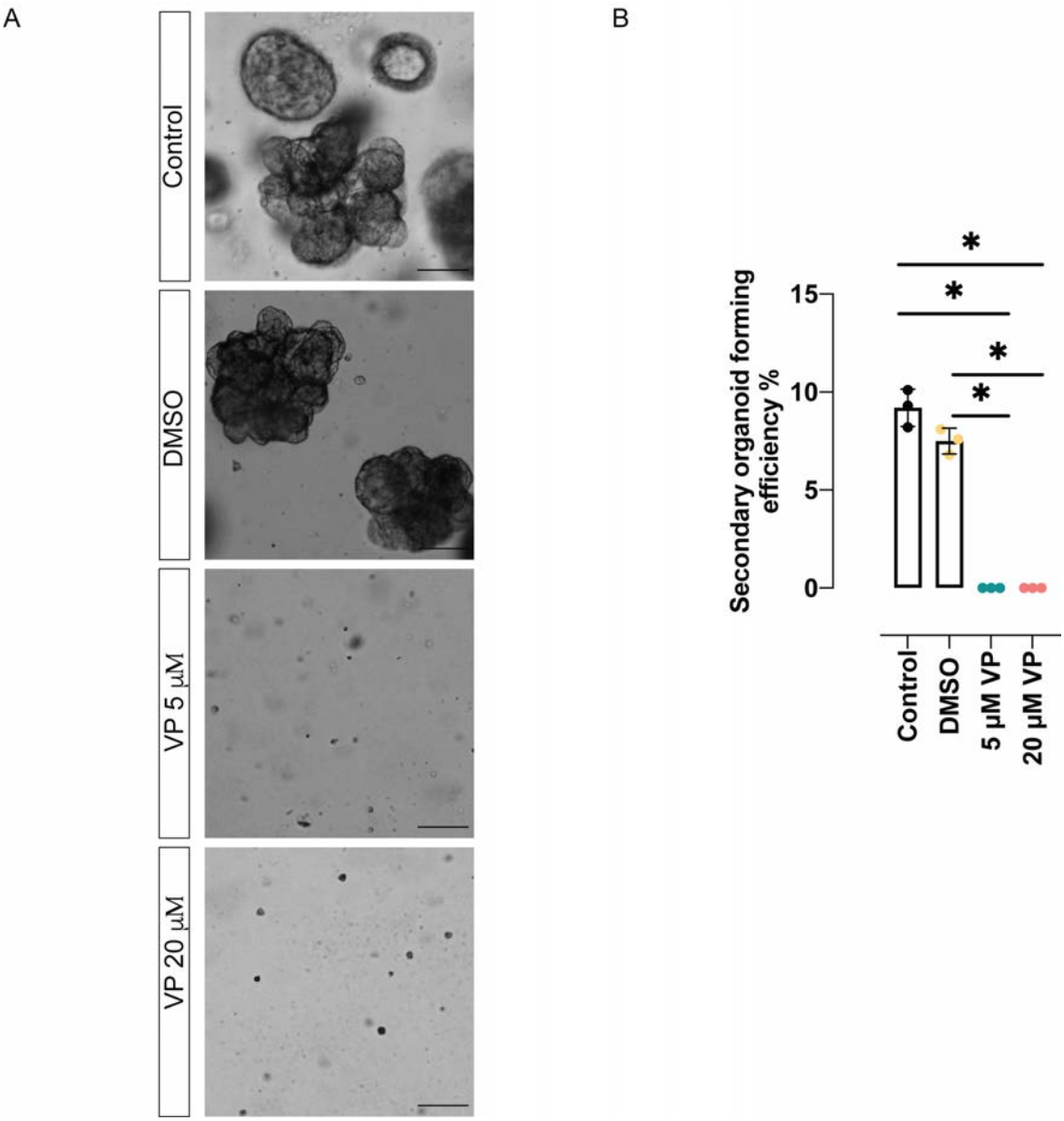

Supplementary Figure 2: Inhibition of YAP nuclear activity inhibits secondary organoid formation. Relative to Figure 2. (A) Representative picture of secondary organoids derived from organoids treated in the previous passage with DMSO, 5 μM VP, 20 μM VP and control. (B) Quantification at the end of the passage of the ability of pretreated cells to form secondary organoids, measured as Organoid forming efficiency OFE%. Data are represented as the mean ± SEM (B). (B) One-way ANOVA *p<0.05, **p<0.01, ***p<0.001, ****p<0.0001.

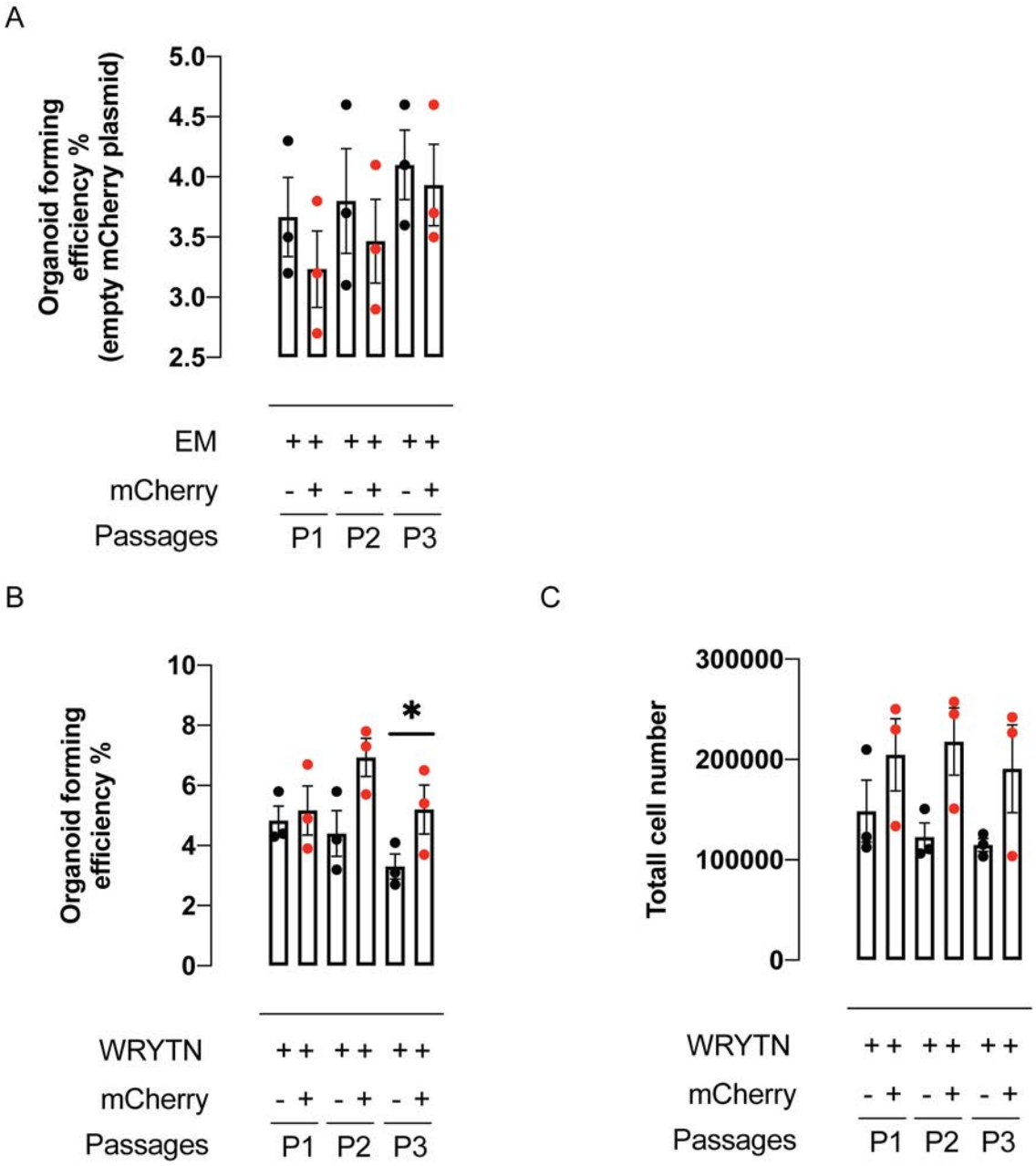

Supplementary Figure 3: YAP overexpression in human salivary gland-derived cells increases their self-renewal potential. Relative to Figure 4. (A) Organoid forming efficiency of human salivary gland cells transduced with empty mCherry plasmid showing no differences in growth between mCherry+ and mCherry-. (B)(C) Quantification of secondary and tertiary organoids (B) and total cell numbers (C) of human salivary gland cells transduced with pGAMA-YAP and cultured in Wnt enriched media (WRYTN). Red dots= mCherry+; Black Dots= mCherry-. Data are represented as the mean ± SEM (A)(B)(C). (B)Two-way ANOVA. *p<0.05, **p<0.01, ***p<0.001, ****p<0.0001.

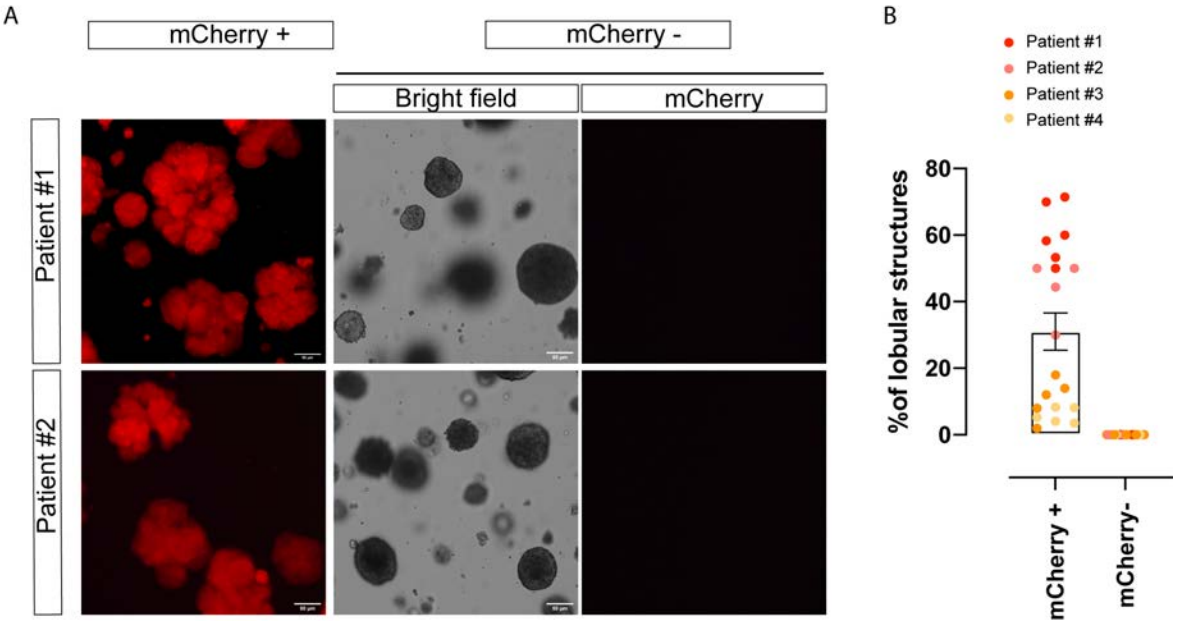

Supplementary Figure 4: YAP overexpression in human salivary gland derived cells promotes branching morphogenesis. Relative to Figure 4. (A) Representative picture of mCherry+ YAP^{OE} overexpressing human salivary gland organoids cultured in EM at the end of passage 1 (P1). YAP^{OE} organoids show branched/lobular phenotype compare to mCherry- derived organoids that show instead a spherical phenotype. (B) Quantification of branched organoids at the end of P1 in 4 different cultures derived from 4 different patients (each color=one patient). % of branched organoids are calculated per well (each dot=1 well).

$$\%\boldsymbol{of\ branched\ organoids} = \frac{\boldsymbol{number\ of\ branched\ organoids\ per\ well}}{\boldsymbol{total\ number\ of\ organoids\ per\ well}} * \mathbf{100}$$

Data are represented as mean ± SEM. (B) T-Test. *p<0.05, **p<0.01, ***p<0.001, ****p<0.0001.

A

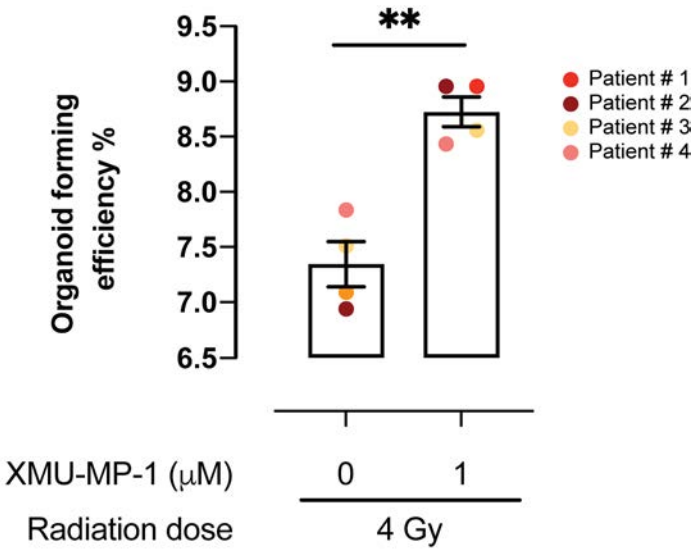

Supplementary Figure 5: Chemical inhibition of MST1/2 kinases improves salivary gland organoid irradiation response. Relative to Figure 5. (A) Organoid forming efficiency of hSG derived cells upon radiation treatment (4 Gy) and inhibition of MST1/2 kinase by the use of XMU-MP1 (1 μM). Each color represents a culture derived from a different patient (n=4). Data are represented as the mean ± SEM. Two-way ANOVA (mixed model). *p<0.05, **p<0.01, ***p<0.001, ****p<0.0001.